Am J Cancer Res 2023;13(3):1091-1102
www.ajcr.us /ISSN:2156-6976/ajcr0147687

Original Article

Subtype-based analysis of cell-in-cell structures in non-small cell lung cancer

Yuexian Wei[1,2,3*], Zubiao Niu[2,3*], Xinyu Hou[4*], Mengzhe Liu[1,2,3*], Yuqi Wang[1,2,3*], Yongan Zhou[5*], Chenxi Wang[2,3], Qunfeng Ma[6], Yichao Zhu[2,3], Xinyue Gao[2,3], Peiyun Li[7], Shuo Gao[7], Sibo Zhan[7], Zi Yang[7], Yanhong Tai[8], Qiuju Shao[9], Jianlin Ge[1], Jilei Hua[1], Lihua Gao[2,3], Qiang Sun[2,3], Hong Jiang[1], Hongyan Huang[4]

[1]College of Life Science and Bioengineering, School of Science, Beijing Jiaotong University, Beijing 100044, China; [2]Laboratory of Cell Engineering, Beijing Institute of Biotechnology, Beijing 100071, China; [3]Research Unit of Cell Death Mechanism, Chinese Academy of Medical Sciences (2021RU008), Beijing 100071, China; [4]Department of Oncology, Beijing Shijitan Hospital of Capital Medical University, Beijing 100038, China; [5]Department of Thoracic Surgery, The Second Affiliated Hospital of Air Force Military Medical University, Xi'an 710032, Shaanxi, China; [6]Department of Thoracic Surgery, The Fifth Medical Center of Chinese PLA General Hospital, Beijing 100071, China; [7]School of Science, Beijing Jiaotong University, Beijing 100044, China; [8]Department of Pathology, The Fifth Medical Center of Chinese PLA General Hospital, Beijing 100071, China; [9]Department of Radiotherapy, The Second Affiliated Hospital of Air Force Military Medical University, Xi'an 710032, China. [*]Equal contributors.

Received November 11, 2022; Accepted February 16, 2023; Epub March 15, 2023; Published March 30, 2023

Abstract: Lung cancer is ranked as the leading cause of cancer-related death worldwide, and the development of novel biomarkers is helpful to improve the prognosis of non-small cell lung cancer (NSCLC). Cell-in-cell structures (CICs), a novel functional surrogate of complicated cell behaviors, have shown promise in predicting the prognosis of cancer patients. However, the CIC profiling and its prognostic value remain unclear in NSCLC. In this study, we retrospectively explored the CIC profiling in a cohort of NSCLC tissues by using the "Epithelium-Macrophage-Leukocyte" (EML) method. The distribution of CICs was examined by the Chi-square test, and univariate and multivariate analyses were performed for survival analysis. Four types of CICs were identified in lung cancer tissues, namely, tumor-in-tumor (TiT), tumor-in-macrophage (TiM), lymphocyte-in-tumor (LiT), and macrophage-in-tumor (MiT). Among them, the latter three constituted the heterotypic CICs (heCICs). Overall, CICs were more frequently present in adenocarcinoma than in squamous cell carcinoma (P = 0.009), and LiT was more common in the upper lobe of the lung compared with other lobes (P = 0.020). In univariate analysis, the presence of TiM, heCIC density, TNM stage, T stage, and N stage showed association with the overall survival (OS) of NSCLC patients. Multivariate analysis revealed that heCICs (HR = 2.6, 95% CI 1.25-5.6) and lymph node invasion (HR = 2.6, 95% CI 1.33-5.1) were independent factors associated with the OS of NSCLC. Taken together, we profiled the CIC subtypes in NSCLC for the first time and demonstrated the prognostic value of heCICs, which may serve as a type of novel functional markers along with classical pathological factors in improving prognosis prediction for patients with NSCLC.

Keywords: Cell-in-cell structures, lung cancer, prognosis, NSCLC, functional pathology

Introduction

Lung cancer is the most common cancer and ranks first in terms of cancer-related deaths worldwide. It is also the leading cause of cancer-related deaths among men and women in China. Non-small cell lung cancer (NSCLC), accounting for more than 80% of all lung cancer cases, is mainly divided into two histological subtypes, including adenocarcinoma (ADC) and squamous cell carcinoma (SCC) [1, 2]. Although surgery and systemic adjuvant therapy prolong the overall survival of patients with lung cancer, disease progression and distant metastasis are inevitable in some patients, even in those who undergo radical resection at a rather early stage. Generally, the 5-year survival rate of NSCLC is approximately 18% [3, 4]. However, a number of patients exhibit an overall survival longer than the average. The specific molecular mechanism underlying the different prognoses in NSCLC has not yet been deter-

mined, and the development of novel biomarkers to predict the prognosis of NSCLC is needed.

Cell-in-cell structures (CICs) are defined as unique structures with one or more cells enclosed within another cell [5, 6], which is prevalent in various human cancer tissues [7, 8]. The formation of CICs is a finely regulated process that is controlled by a set of core elements [9], including adherens junctions [10-12], contractile actomyosin [13, 14], and mechanical ring [15]. Molecules targeting these core elements, such as p53, CD44, TRAIL, 4.1N, IL-8, IL-6, CDKN2a, and cholesterol, are important regulators of CIC formation [16-24]. The formation of CICs is believed to be a death program [25], leading to the death of either the internalized cells in an acidified lysosome [26, 27] or the outer host cells under certain circumstances [23]. Therefore, CICs have been implicated in many important processes, such as immune homeostasis [28], viral transmission and pathogenesis [29-32], and genomic instability and tumor evolution [18, 19, 33]. According to the types of cells involved in the formation, CICs are categorized into two common subgroups, namely, homotypic CICs (HoCICs, formed between tumor cells) and heterotypic CICs (HeCICs, formed between tumor cells and other types of cells, such as immune cells) [34-36]. In terms of heCICs, there is more than one kind of subtype in tumor tissues where different immune cells are involved in the formation of CICs [8, 37]. Currently, as novel functional surrogates of complicated cell behaviors, CICs have been reported to predict patient prognosis for multiple cancers [35, 37-42]. However, the CIC profiling and its prognostic value remain unclear for NSCLC.

This retrospective study aimed to profile the CIC subtypes in a cohort of tumor tissues from patients with NSCLC and to explore their prognostic values for NSCLC.

Materials and methods

Study population

We conducted a retrospective analysis of 220 patients with histologically confirmed NSCLC from May 2014 to March 2019. Among the 220 patients, 145 cases were from the Fifth Medical Center of Chinese PLA General Hospital (Beijing, China) or the Second Affiliated Hospital of Air Force Military Medical University (Xi'an, China), and 75 cases were from commercial tumor microarray (TMA) (HLugA150CS02, XT15-045, Shanghai Outdo Biotech Co. Ltd.). The inclusion criteria include: a. received radical surgery; b. had the complete clinical and follow-up information. The exclusion criteria included: a. distant metastasis was found before or during the operation; b. patients who received treatment prior to radical surgery.

Clinical data such as age, sex, tumor size, histology, TNM stage, and survival data were collected. The follow-up data were obtained from outpatient visit or telephone follow-ups. The OS was defined as the time from the day of diagnosis to the day of the last visit or death. The ethics committee of the Fifth Medical Center of Chinese PLA General Hospital and the Second Affiliated Hospital of Air Force Military Medical University approved the study and granted a waiver of informed consent, considering the retrospective nature of the study.

Immunostaining and image processing

Formalin-fixed and paraffin-embedded tissue specimens were cut into 5-μm-thick sections, mounted on poly-lysine-coated slides routinely. The "Epithelium-Macrophage-Leukocyte" (EML) method was used to subtype CICs as previously reported [7]. In brief, samples were first stained with antibody against CD45 (mouse mAb from Boster, BM0091) at a dilution of 1:400 by Opal Multiplex tissue staining kit (Perkin Elmer, NEL791001KT) according to the standard protocol provided, and CD45 molecules were eventually labeled with Cyanine 5 fluorophore. Slides were then incubated with mixed antibodies against E-cadherin (mouse mAb from BD Biosciences, 610181) and CD68 (rabbit pAb from Proteintech, 25747-1-AP), followed by secondary antibodies of Alexa Fluor 568 anti-rabbit antibody (Invitrogen, A11036) and Alexa Fluor 488 anti-mouse antibody (Invitrogen, A11029). All slides were counterstained with DAPI to show nuclei and mounted with Antifade reagent (Invitrogen, Carlsbad, CA) and cover slips. Multispectral images were taken with TMA modules of VectraR Automated Imaging System (Perkin Elmer) by a 20× objective lens. Nuance system (Perkin Elmer) was used to build libraries of each spectrum (DAPI, FITC, TRITC, and Cy5) and unmix multispectral imag-

Table 1A. The clinical pathological characteristics of patients in this study

	Cancer tissues n (%)	Para-carcinoma n (%)	Normal tissues n (%)	Valid cancer tissues n (%)
Sample number	220	220	142	163
Age (years)				156
<60	101 (45.9)	101 (45.9)	67 (47.2)	77 (49.4)
≥60	108 (49.1)	108 (49.1)	68 (47.9)	79 (50.6)
NA	11 (5.0)	11 (5.0)	7 (4.9)	
Sex				157
Male	135 (61.4)	135 (61.4)	96 (67.6)	95 (60.5)
Female	75 (34.1)	75 (34.1)	39 (27.5)	62 (39.5)
NA	10 (4.5)	10 (4.5)	7 (4.9)	
Type				162
Adenocarcinoma	112 (50.9)	112 (50.9)	49 (34.5)	93 (57.4)
Squamous carcinoma	64 (29.1)	64 (29.1)	64 (45.1)	41 (25.3)
Others	39 (17.7)	39 (17.7)	27 (19.0)	28 (17.3)
NA	5 (2.3)	5 (2.3)	2 (1.4)	
Location				152
Upper	113 (51.4)	113 (51.4)	75 (52.8)	83 (50.9)
Middle	20 (9.1)	20 (9.1)	15 (10.6)	16 (9.8)
Lower	65 (29.5)	65 (29.5)	37 (26.1)	53 (32.5)
NA	22 (10.0)	22 (10.0)	15 (10.6)	
TNM stage				148
I + II	114 (51.8)	114 (51.8)	68 (47.9)	92 (62.2)
III + IV	70 (31.8)	70 (31.8)	51 (35.9)	56 (37.8)
NA	36 (16.4)	36 (16.4)	23 (16.2)	
T stage				157
T1 + T2	149 (67.7)	149 (67.7)	86 (60.6)	124 (79.0)
T3 + T4	52 (23.6)	52 (23.6)	40 (28.2)	33 (21.0)
NA	19 (8.6)	19 (8.6)	16 (11.3)	
N stage				157
N0	92 (41.8)	92 (41.8)	52 (36.6)	75 (47.8)
N1-N3	109 (49.5)	109 (49.5)	74 (52.1)	82 (52.2)
NA	19 (8.6)	19 (8.6)	16 (11.3)	
Histology grade				122
I	29 (13.2)	29 (13.2)	16 (11.3)	26 (21.3)
II	86 (39.1)	86 (39.1)	35 (24.6)	76 (62.3)
III	26 (11.8)	26 (11.8)	16 (11.3)	20 (16.4)
NA	79 (35.9)	79 (35.9)	75 (52.8)	
Survival time				163
<43	86 (39.1)	86 (39.1)	61 (43.0)	84 (51.5)
≥43	84 (38.2)	84 (38.2)	34 (23.9)	79 (48.5)
NA	50 (22.7)	50 (22.7)	47 (33.1)	

NA: not available.

es with high contrast and accuracy. InForm automated image analysis software (Perkin Elmer) was used for batch analysis of multispectral images based on specified algorithms.

Quantification of CICs in tissue

CICs were quantified as previously described [37]. Briefly, CICs were first identified from a composite image with multiple fluorescent

Table 1B. The clinical pathological characteristics of patients in this study

Characteristics	No (%), n = 163
Age (years)	
<60	77 (47.2)
≥60	79 (48.5)
Unknown	7 (4.3)
Sex	
Male	95 (58.3)
Female	62 (38.0)
Unknown	6 (3.7)
Histology	
ADC	93 (57.1)
SCC	41 (25.2)
Others	28 (17.2)
Unknown	1 (0.6)
Location	
Upper lobe	83 (50.9)
Middle lobe	16 (9.8)
Lower lobe	53 (32.5)
Unknown	11 (6.7)
TNM stage	
I	53 (32.5)
II	39 (23.9)
III	56 (34.4)
Unknown	16 (9.8)
T stage	
T1	30 (18.4)
T2	94 (57.7)
T3	26 (16.0)
T4	7 (4.3)
Unknown	6 (3.7)
LN invasion	
No	75 (46.0)
Yes	82 (50.3)
Unknown	6 (3.7)
Histology grade	
I	26 (16.0)
II	76 (46.6)
III	20 (12.3)
Unknown	41 (25.2)

LN: lymph node; unknown: the information is not available.

channels merged together and then confirmed in an individual fluorescent channel for CIC subtyping. A cellular structure where one or more cells are fully enclosed inside another cell was scored as CIC.

The density of CICs was employed to represent the quantity of CICs in each sample as reported previously [43]. Firstly, eight to ten fields were selected randomly considering the homogeneity and representativeness. Secondly, the number of CICs in each field was counted by two individual pathologists blind to clinical data. Finally, the density of CICs was calculated as the total number of CICs standardized by the total area of all the fields selected.

Statistical analysis

The relationship between the clinicopathological characteristics of the patients and CICs was analyzed using the Chi-squared test or Fisher exact test, appropriately. Kaplan-Meier method was used to plot survival curves and the log-rank test was used to compare the differences. Cox regression model was conducted to investigate the prognostic significance. All statistical analyses were performed using GraphPad Prism 6.0. For all these analyses, P value <0.05 was considered significant. Two-sided tests were used throughout the study.

Results

Patient characteristics

In total, 163 out of 220 patients with qualified EML staining were eventually enrolled in this retrospective study, with a median follow-up of 41 months (range, 1-96 months). The baseline characteristics of the patients are summarized in **Table 1A**, **1B**. The median age was 59 years (20-84 years). Among patients with relevant information, most of them were male (95 out of 163, 58.3%) and at T2 stage (57.7%). A total of 53 patients (32.5%) were in TNM stage I, 39 (23.9%) were in stage II, and 56 (34.4%) were in stage III. The histopathological types were primarily adenocarcinoma (57.1%) and squamous cell carcinoma (25.2%).

CIC profiling in NSCLC

A total of 220 lung cancer tissue samples, 220 paired para-carcinoma tissues, and 142 paired normal tissues were stained by using the EML method. Among the 220 tumor specimens, 163 specimens were effectively stained and analyzed in this study. CICs were present in 101 tumor tissues with an average density of 1.56 CICs/mm^2 (range, 0.11-5.88 CICs/mm^2) (**Figure**

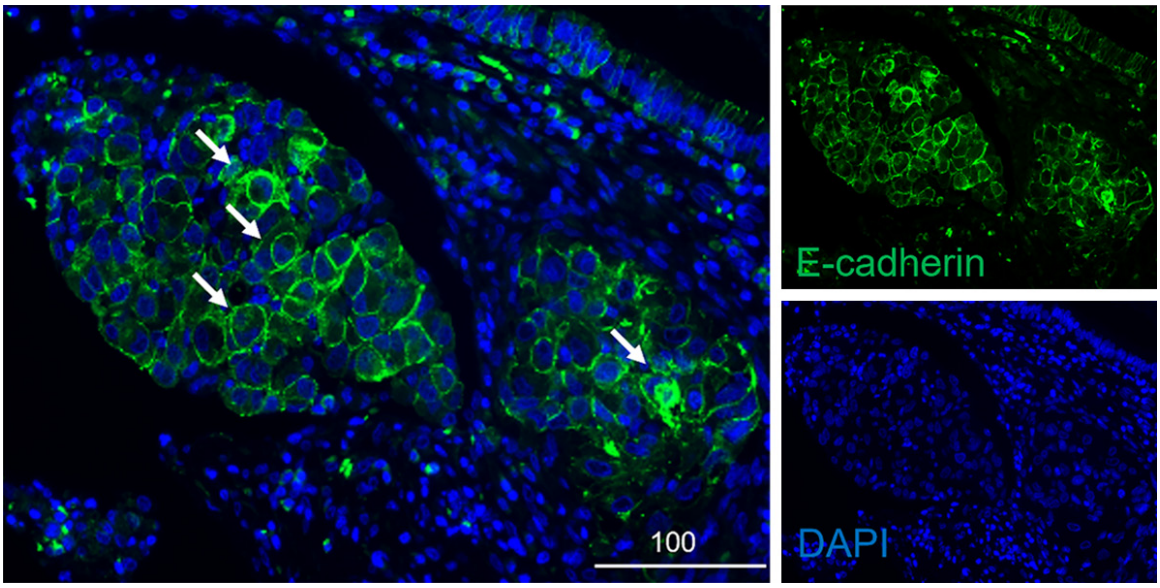

Figure 1. Cell-in-cell structures in lung cancer. Right panels show channeled images of the left merged image. Scale bar: 100 μm. Arrows indicate cell-in-cell structures.

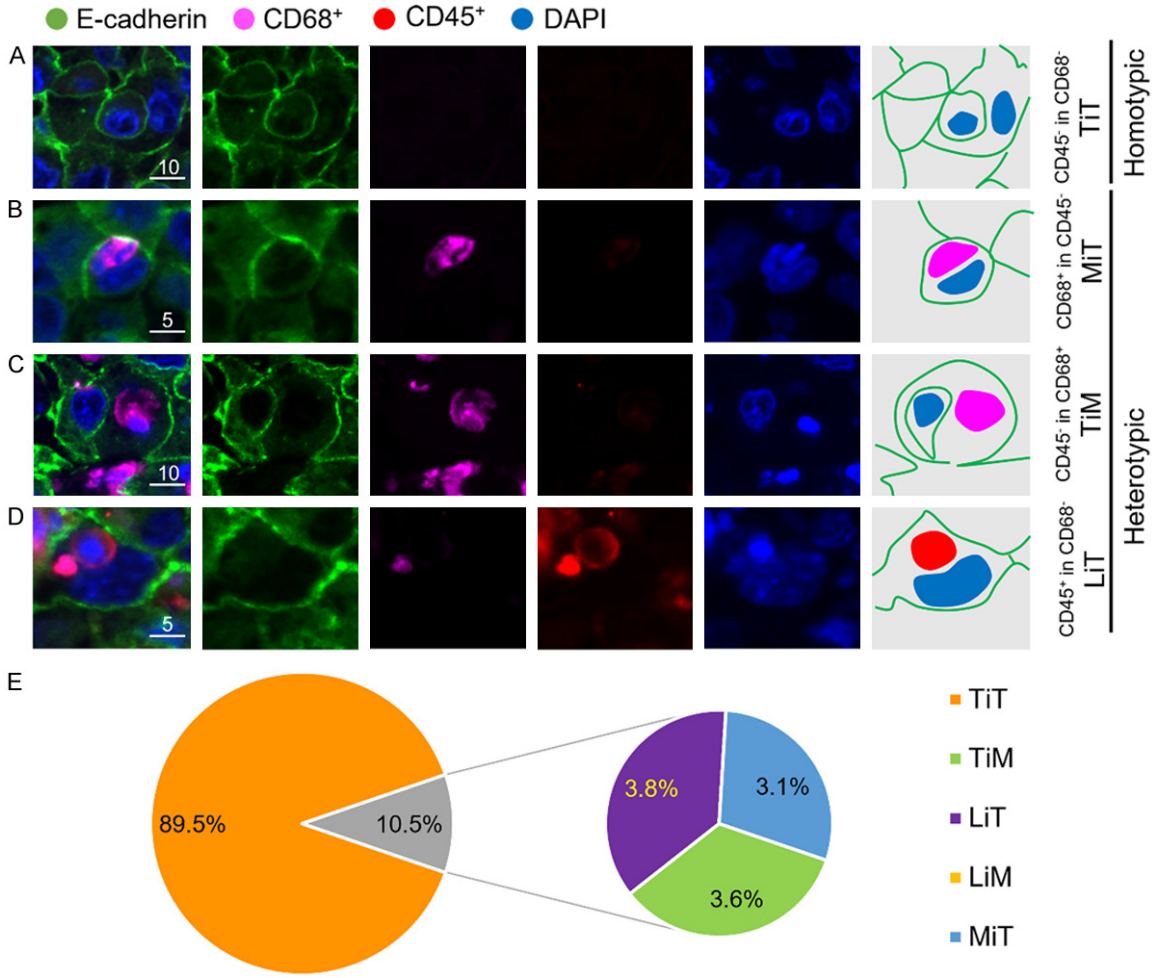

Figure 2. Subtype profiling of cell-in-cell structures in lung cancer. A-D. Representative images for four CIC subtypes as indicated. Right panels of pictures demonstrate the schematic structure for each CIC subtype. Scale bar: 5 or 10 μm as indicated. E. Distribution of four CIC subtypes across lung cancer tissues in all patients (n = 163).

Table 2. Association of CIC subtypes with clinicopathological characteristics

	N/n (%)	TiT			TiM			LiT			MiT			HeCICs			oCICs		
		Low	High	*P*	Yes	No	*P*	Yes	No	P	Yes	No	*P*	Low	High	*P*	Low	High	*P*
Age (years)	156			0.854			0.077			0.39			0.091			0.564			0.679
<60	77 (49.4)	68 (88.3)	9 (11.7)		3 (3.9)	74 (96.1)		4 (5.2)	73 (94.8)		5 (6.5)	72 (93.5)		68 (88.3)	9 (11.7)		68 (88.3)	9 (11.7)	
≥60	79 (50.6)	69 (87.3)	10 (12.7)		0 (0.0)	79 (100.0)		2 (2.5)	77 (97.5)		1 (1.3)	78 (98.7)		68 (86.1)	11 (13.9)		72 (91.1)	7 (8.9)	
Sex	157			0.803			0.16			0.246			0.246			0.074			0.356
Male	95 (60.5)	83 (87.4)	12 (12.6)		3 (3.2)	92 (96.8)		5 (5.3)	90 (94.7)		5 (5.3)	90 (94.7)		81 (85.3)	14 (14.7)		82 (86.3)	13 (13.7)	
Female	62 (39.5)	55 (88.7)	7 (11.3)		0 (0.0)	62 (100.0)		1 (1.6)	61 (98.4)		1 (1.6)	61 (98.4)		56 (90.3)	7 (11.3)		59 (95.2)	3 (4.8)	
Type	162			0.062			0.237			0.777			0.163			0.479			0.009
ADC	93 (57.4)	78 (83.9)	15 (16.1)		1 (1.1)	92 (98.9)		3 (3.2)	90 (96.7)		5 (5.4)	88 (94.6)		76 (81.7)	17 (18.3)		82 (88.2)	11 (11.8)	
SCC	41 (25.3)	39 (95.1)	2 (4.9)		2 (4.9)	39 (95.1)		2 (4.9)	39 (95.1)		1 (2.4)	40 (97.6)		39 (95.1)	2 (4.9)		37 (90.2)	4 (9.8)	
Others	28 (17.3)	26 (92.9)	2 (7.1)		1 (3.6)	27 (96.4)		1 (3.6)	27 (96.4)		0 (0.0)	28 (100.0)		27 (96.4)	1 (3.6)		26 (92.9)	2 (7.1)	
Location	152			0.68			0.501			0.02			0.488			0.962			0.665
Upper	83 (50.9)	73 (88.0)	10 (12.0)		1 (1.2)	82 (98.8)		6 (7.2)	77 (92.8)		4 (4.8)	79 (95.2)		72 (86.7)	11 (13.3)		74 (89.2)	9 (10.8)	
Middle	16 (9.8)	14 (87.5)	2 (12.5)		1 (6.3)	15 (93.8)		0 (0.0)	16 (100.0)		0 (0.0)	16 (100.0)		15 (93.8)	1 (6.3)		16 (100.0)	0 (0.0)	
Lower	53 (32.5)	46 (86.8)	7 (13.2)		2 (3.8)	51 (96.2)		0 (0.0)	53 (100.0)		2 (3.8)	51 (96.2)		45 (84.9)	8 (15.1)		45 (84.9)	8 (15.1)	
TNM	148			0.585			0.614			0.534			0.278			0.568			0.707
I + II	92 (62.2)	83 (90.2)	9 (9.8)		2 (2.2)	90 (97.8)		3 (3.3)	89 (96.7)		5 (5.4)	87 (94.6)		82 (89.1)	10 (10.9)		81 (88.0)	11 (12.0)	
III + IV	56 (37.8)	52 (92.9)	4 (7.1)		2 (3.6)	54 (96.4)		3 (5.4)	53 (94.6)		1 (1.8)	55 (98.2)		51 (91.1)	5 (8.9)		51 (91.1)	5 (8.9)	
T stage	157			0.633			0.844			0.791			0.2			0.325			0.483
T1 + T2	124 (79.0)	109 (87.9)	15 (12.1)		3 (2.4)	121 (97.6)		5 (4.0)	119 (96.0)		6 (4.8)	118 (95.2)		107 (86.3)	17 (13.7)		109 (87.9)	15 (12.1)	
T3 + T4	33 (21.0)	30 (90.9)	3 (9.1)		1 (3.0)	32 (97.0)		1 (3.0)	32 (97.0)		0 (0.0)	33 (100.0)		30 (90.9)	3 (9.1)		31 (93.9)	2 (6.1)	
N stage	157			0.231			0.053			0.474			0.076			0.951			0.244
N0	75 (47.8)	64 (85.3)	11 (14.7)		0 (0.0)	75 (100.0)		2 (2.7)	73 (97.3)		5 (6.7)	70 (93.3)		63 (84.0)	12 (16.0)		67 (89.3)	8 (10.7)	
N1-N3	82 (52.2)	75 (91.5)	7 (8.5)		4 (4.9)	78 (95.1)		4 (4.9)	78 (95.1)		1 (1.2)	81 (98.8)		74 (90.2)	8 (9.8)		73 (89.0)	9 (11.0)	
Grade	122			0.424			0.075			0.864			0.592			0.547			0.406
I	26 (21.3)	24 (92.3)	2 (7.7)		2 (7.7)	24 (92.3)		0 (0.0)	26 (100.0)		1 (3.8)	25 (96.2)		25 (96.2)	1 (3.8)		24 (92.3)	2 (7.7)	
II	76 (62.3)	63 (82.9)	13 (17.1)		1 (1.3)	75 (98.7)		3 (3.9)	73 (96.1)		4 (5.3)	72 (94.7)		60 (78.9)	16 (21.1)		65 (85.5)	11 (14.5)	
III	20 (16.4)	17 (85.0)	3 (15.0)		0 (0.0)	20 (100.0)		0 (0.0)	20 (100.0)		0 (0.0)	20 (100.0)		18 (90.0)	2 (10.0)		20 (100.0)	0 (0.0)	

ADC: adenocarcinoma; SCC: squamous cell carcinoma; Grade: histological grade. Tumor-in-tumor (TiT) Low: <1.125 CICs/mm^2, High: ≥1.125 CICs/mm^2; heterotypic CICs (HeCICs) Low: <0.125 CICs/mm^2, High: ≥0.125 CICs/mm^2; overall CICs (oCICs) Low: <1.288 CICs/mm^2, High: ≥1.288 CICs/mm^2; tumor-in-macrophage (TiM), lymphocyte-in-tumor (LiT) and macrophage-in-tumor (MiT), No: 0 CICs/mm^2; Yes: >0 CICs/mm^2. Spearman rank test was used to determine the association between variables.

Table 3. Association of overall survival with clinicopathological parameters and CICs by univariate Cox-regression analysis

Variables	Class	n	HR	95% CI	*P* value	mOS
TiT	High	19	0.541	0.234-1.252	0.151	NA
	Low	144				62
TiM	Yes	4	5.063	1.557-16.468	0.007	13.5
	No	159				78
LiT	Yes	6	1.719	0.540-5.476	0.359	24
	No	157				78
MiT	Yes	6	0.25	0.035-1.800	0.168	NA
	No	157				78
oCICs	High	20	0.526	0.227-1.216	0.133	NA
	Low	143				62
HeCICs	High	17	1.982	1.040-3.777	0.038	33
	Low	146				78
Age (y)	<60	77	1.428	0.885-2.304	0.144	NA
	≥60	79				52
Sex	Male	95	0.709	0.432-1.165	0.175	62
	Female	62				NA
Location	Upper	83	1.148	0.919-1.436	0.225	78
	Middle	16				NA
	Lower	53				NA
Type	ADC	93	1.176	0.879-1.573	0.275	NA
	SCC	41				NA
	Others	28				48
TNM stage	I + II	92	3.226	1.964-5.300	<0.001	NA
	III + IV	56				29
T stage	T1 + T2	124	1.914	1.127-3.250	0.016	NA
	T3 + T4	33				38
N stage	N0	75	3.366	1.998-5.671	<0.001	NA
	N1-N3	82				33
Histology grade	I	26	1.159	0.752-1.786	0.505	78
	II	76				NA
	III	20				NA

ADC: adenocarcinoma; SCC: squamous cell carcinoma; NA: not applicable. Tumor-in-tumor (TiT) Low: <1.125 CICs/mm^2, High: ≥1.125 CICs/mm^2; heterotypic CICs (HeCICs) Low: <0.125 CICs/mm^2, High: ≥0.125 CICs/mm^2; overall CICs (oCICs) Low: <1.288 CICs/mm^2, High: ≥1.288 CICs/mm^2; tumor-in-macrophage (TiM), lymphocyte-in-tumor (LiT) and macrophage-in-tumor (MiT), No: 0 CICs/mm^2; Yes: >0 CICs/mm^2.

1). There were no CICs detected in para-carcinoma or normal lung tissues.

As shown in **Figure 2**, the following four types of CICs were identified in lung cancer tissues: (A) tumor cell in tumor cell (TiT), (B) macrophage in tumor cell (MiT), (C) tumor cell in macrophage (TiM), and (D) lymphocyte in tumor cell (LiT). TiT corresponded to hoCICs, as reported previously [38], while the other three subtypes were considered heCICs. The overall CICs (oCICs) included all kinds of CIC subtypes.

Consistent with our previous reports on CIC subtype profiling, hoCICs were the prevalent subtypes, accounting for 89.5% of the oCICs, and heCICs were much less frequent, accounting for 10.5% of the oCICs in NSCLC. LiT (3.8%), TiM (3.6%), and MiT (3.1%) showed no obvious difference in distribution (**Figure 2E**).

Association between CIC subtypes and clinicopathological variables

Similar to our previous reports on human esophageal squamous cell Carcinoma (ESCC) [43], CIC density, formulated as CIC count per mm^2, was used in this study. Considering that the quantity of one specified heCIC subtype was low in NSCLC, oCICs, TiT, and heCICs were evaluated by density in the subsequent analysis. The patients were then divided into two groups according to the optimized cut-off values selected by the "surv_cutpoint" function of the "survminer" R package for TiT (1.125/mm^2), heCICs (0.125/mm^2), and oCICs (1.288 CICs/mm^2) (Figure S1).

As shown in **Table 2**, oCICs were more frequently present in ADC than in SCC (P = 0.009), and LiT was more common in the upper lobe of the lung compared with other lobes (P = 0.020). However, there was no association between oCICs and sex, location, lymph node status, and TNM stage. Moreover, no association was detected between TiT and all the variables examined in this study.

Association between CIC subtypes and survival

In univariate analysis with Cox regression model, the presence of TiM, heCIC density, TNM stage, T stage, and N stage were found to be significantly associated with the overall sur-

Table 4. Multivariate Cox regression analysis of overall survival

Characteristics	Class	n	HR	95% CI	*P* value
TiM	Yes	3	2.0	0.57-7.1	0.273
	No	154			
HeCICs	Low	136	2.6	1.25-5.6	0.011
	High	20			
TNM stage	I + II	92	1.7	0.88-3.4	0.112
	III + IV	56			
T stage	T1 + T2	124	1.5	0.81-2.7	0.205
	T3 + T4	33			
N stage	N0	75	2.6	1.33-5.1	0.005
	N1-N3	82			

Heterotypic CICs (HeCICs) Low: <0.125 CICs/mm^2, High: ≥0.125 CICs/mm^2; tumor-in-macrophage (TiM), No: 0 CICs/mm^2; Yes: >0 CICs/mm^2. Spearman rank test was used to determine the association between variables.

vival (OS) of patients with NSCLC (**Table 3**, Table S1). Moreover, multivariate analysis showed that heCIC density (HR = 2.6, 95% CI 1.25-5.6) and lymph node invasion (HR = 2.6, 95% CI 1.33-5.1) were independent factors associated with the OS of patients with NSCLC (**Table 4**). Besides, patients with higher density of heCICs exhibited significantly shorter OS time compared with those with lower density of heCICs (mOS: 33 vs. 78 months, $P = 0.035$), to which TiM positively contributed, given that TiM alone profoundly differentiated patient survival (mOS: 13.5 vs. 78 months, $P = 0.0033$) with limited number of patients (**Figure 3**). In contrast, high density of TiT or oCICs only appeared to favor good prognosis, considering that the difference was not statistically significant (**Figure 3**).

Discussion

In this study, we explored the subtyped CIC profile in NSCLC and identified four subtypes of CICs in lung cancer. Our study revealed that more heCICs were adversely associated with the survival time in patients with NSCLC, suggesting that subtyped CICs can be used in predicting the prognosis of patients with NSCLC, along with other classic clinicopathological factors.

CICs have been documented in various types of solid malignancies where both hoCICs and heCICs are formed. With the development of methods to identify the cell types involved in CICs, different CIC subtypes have been demonstrated [7]. Analysis of the relationship between CIC subtypes and prognosis revealed the distinct prediction value of profiled CIC subtypes for the prognosis of heterogeneous cancers [37, 38, 43]. In this study, we explored the subtyped CIC profiling in NSCLC for the first time and demonstrated the value of heCICs in prognosis prediction for patients with NSCLC, which is consistent with our previous findings in pancreatic ductal adenocarcinoma [37]. We reinforced the concept of heCICs as a promising functional pathological parameter to read out the complicated outcome of intercellular interactions within the tumor microenvironment and differential prognosis of patients after radical surgery.

In line with previous reports [37, 38, 43], homotypic CICs were still the dominant subtype of the oCICs in NSCLC tissue. The performance of TiT in predicting prognosis was also evaluated. Our results indicated that TiT was a merely weak predictor, evidenced by the fact that the association of TiT with OS was identified in univariate analysis but failed to be confirmed in subsequent multivariate analysis. As for the value of TiT in prognosis prediction across different types of malignancies, it remains inconsistent in the context of specific types of tumor. The increased number of TiTs indicates poor prognosis in pancreatic ductal carcinoma as well as in head and neck carcinoma but prolongs survival time in breast cancer. The underlying mechanism should be studied further by investigating more tumor types. In comparison with hoCICs, heCICs accounted for a much lower proportion of oCICs. Notably, the contribution to prognosis prediction was remarkably greater for heCICs than for TiTs in this study, which suggests that CIC subtype analysis is necessary when CICs are considered to be used.

Although heCICs have been identified as an adverse prognostic factor in early breast cancer [38] and pancreatic cancer [37] previously and in NSCLC in this study, the method of identifying and quantifying CIC subtype merits more exploration. The EML staining was established [7] and previously used by our group in CIC subtyping of several tumor tissues; it was again proven to be successful in NSCLC in this study. These results indicate that EML staining is a reliable method for CIC subtyping in tumors,

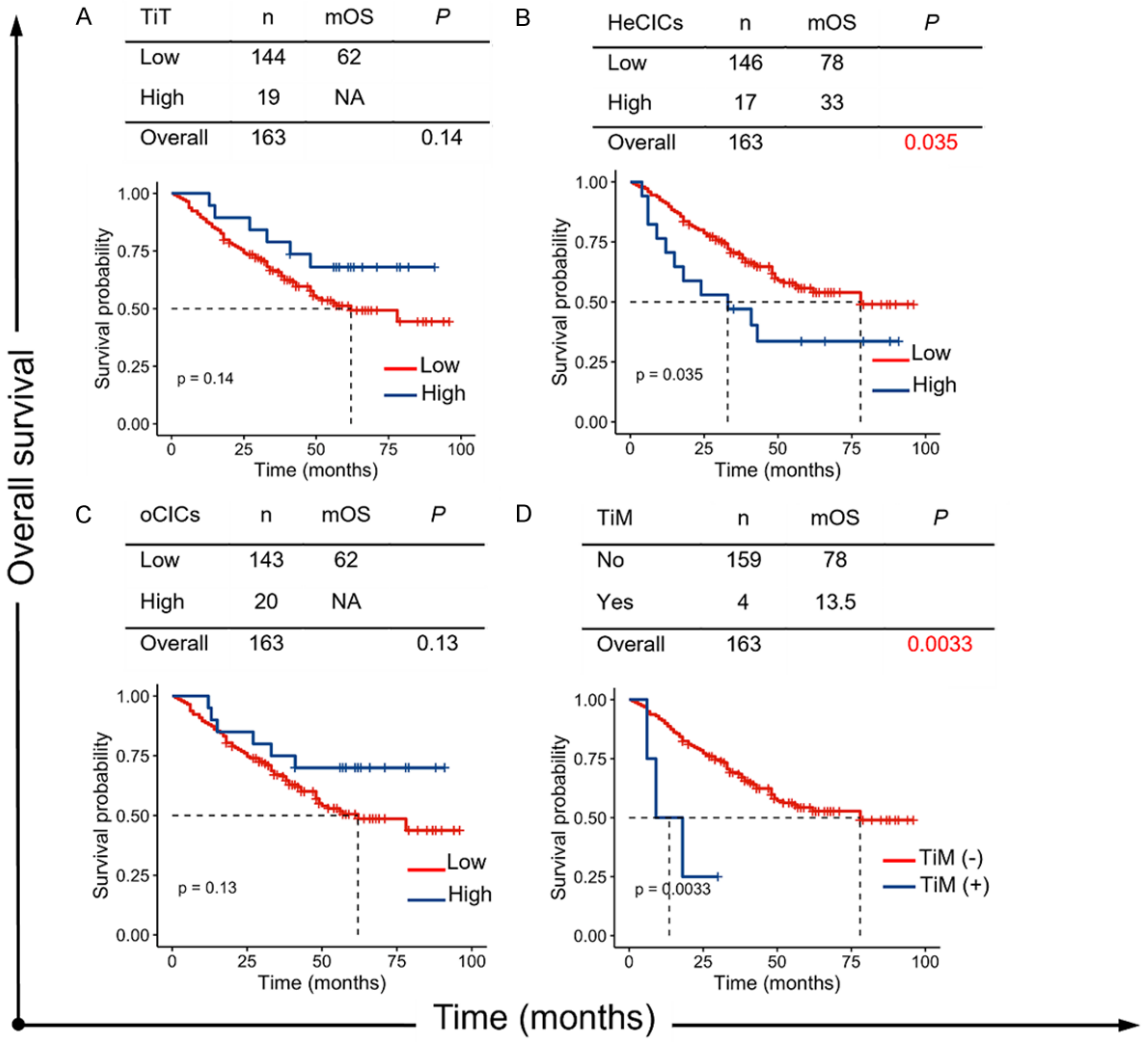

Figure 3. Impacts of CICs on overall survival (OS) of lung cancer patients. Kaplan-Meier plotting for OS curves of (A) Tumor-in-tumor (TiT), (B) Heterotypic CICs (HeCICs), (C) Overall CICs (oCICs), and (D) Tumor-in-macrophage (TiM). TiT Low: <1.125 CICs/mm^2, High: ≥1.125 CICs/mm^2; HeCICs Low: <0.125 CICs/mm^2, High: ≥0.125 CICs/mm^2; oCICs Low: <1.288 CICs/mm^2, High: ≥1.288 CICs/mm^2; TiM (-): 0 CICs/mm^2; TiM (+): >0 CICs/mm^2.

although more molecular markers should be tried or added in multiplex staining in the future to identify more detailed CIC subtypes. In terms of CIC quantification, we have initially counted the number of CICs in confined views, and then recently, we have tried to introduce CIC density into the prognostic value analysis of CICs. Similar to our previous report on ESCC [43], heCICs in this study were also evaluated by density. The results indicated that a higher density of heCICs was significantly associated with shortened OS of patients with NSCLC both in univariate and subsequent multivariate analyses. In other words, there was a direct association between heCICs and significantly increased death hazard of the patient (HR = 2.6, P = 0.011). The result indicates that CIC density may also be an optional parameter to quantify the CICs in tumor tissues.

When looking into the constitution of heCICs, the proportion of each subtype was similar. Meanwhile, we found that among the three heCIC subtypes identified in this study, TiM was the only one that showed influence on patients' survival time in univariate analysis, suggesting that TiM is a major contributor of prognostic power of heCICs. Coincidently, the formation of TiM with tumor cell engulfed by macrophage was previously reported to be associated with

prognosis in breast cancer [38], suggesting an important role of macrophages in tumor malignancy.

There are several limitations in this study. First, the retrospective nature and the limited sample size of this study make bias inevitable. Second, the lack of information about gene mutation in tumor tissue, adjuvant therapy, or disease progression may have impaired the accuracy of assessment of prognosis prediction value for CIC subtypes or other clinicopathological factors. Finally, the role that CIC subtype profiling played in predicting prognosis between ADC and SCC, which show distinct characteristics, was not compared due to the limited sample size in this study.

In summary, this study identified the CIC subtype profile in NSCLC for the first time. We found that heCICs were associated with adverse prognosis for patients with NSCLC, suggesting that CIC subtype profiling could provide more information about tumor malignancy and prognosis.

Acknowledgements

This research was funded by Beijing Municipal Natural Science Foundation (KZ202110025-029), the National Natural Science Foundation of China (31970685), and Beijing Municipal Administration of Hospitals Incubating Program (PX2021033), the National Key R&D Program of China (2022YFC3600100).

The TMA was purchased from Shanghai Outdo Biotech Co. Ltd., which was part of National Human Genetic Resources Sharing Service Platform, and approved to provide TMA with license No.: 2005DKA21300. Informed consent was obtained from all subjects involved in the study. The samples were collected under high ethical standards with the donor being informed completely.

Disclosure of conflict of interest

None.

Address correspondence to: Qiang Sun, Laboratory of Cell Engineering, Beijing Institute of Biotechnology, Beijing 100071, China. E-mail: sunq@bmi.ac.cn; Hong Jiang, College of Life Science and Bioengineering, School of Science, Beijing Jiaotong University, Beijing 100044, China. E-mail: jhong@bjtu.edu.cn; Hongyan Huang, Department of Oncology, Beijing Shijitan Hospital of Capital Medical University, Beijing 100038, China. E-mail: huangh1975@mail.ccmu.edu.cn

References

[1] Molina JR, Yang P, Cassivi SD, Schild SE and Adjei AA. Non-small cell lung cancer: epidemiology, risk factors, treatment, and survivorship. Mayo Clin Proc 2008; 83: 584-594.

[2] Herbst RS, Morgensztern D and Boshoff C. The biology and management of non-small cell lung cancer. Nature 2018; 553: 446-454.

[3] Hirsch FR, Scagliotti GV, Mulshine JL, Kwon R, Curran WJ Jr, Wu YL and Paz-Ares L. Lung cancer: current therapies and new targeted treatments. Lancet 2017; 389: 299-311.

[4] Visbal AL, Leighl NB, Feld R and Shepherd FA. Adjuvant chemotherapy for early-stage non-small cell lung cancer. Chest 2005; 128: 2933-2943.

[5] Huang H, Chen Z and Sun Q. Mammalian cell competitions, cell-in-cell phenomena and their biomedical implications. Curr Mol Med 2015; 15: 852-860.

[6] Fais S and Overholtzer M. Cell-in-cell phenomena in cancer. Nat Rev Cancer 2018; 18: 758-766.

[7] Huang H, Chen A, Wang T, Wang M, Ning X, He M, Hu Y, Yuan L, Li S, Wang Q, Liu H, Chen Z, Ren J and Sun Q. Detecting cell-in-cell structures in human tumor samples by E-cadherin/CD68/CD45 triple staining. Oncotarget 2015; 6: 20278-20287.

[8] Mlynarczuk-Bialy I, Dziuba I, Sarnecka A, Platos E, Kowalczyk M, Pels KK, Wilczynski GM, Wojcik C and Bialy LP. Entosis: from cell biology to clinical cancer pathology. Cancers (Basel) 2020; 12: 2481.

[9] Niu Z, He M and Sun Q. Molecular mechanisms underlying cell-in-cell formation: core machineries and beyond. J Mol Cell Biol 2021; 13: 329-334.

[10] Wang M, Ning X, Chen A, Huang H, Ni C, Zhou C, Yu K, Lan S, Wang Q, Li S, Liu H, Wang X, Chen Z, Ma L and Sun Q. Impaired formation of homotypic cell-in-cell structures in human tumor cells lacking alpha-catenin expression. Sci Rep 2015; 5: 12223.

[11] Sun Q, Cibas ES, Huang H, Hodgson L and Overholtzer M. Induction of entosis by epithelial cadherin expression. Cell Res 2014; 24: 1288-1298.

[12] Wang C, Chen A, Ruan B, Niu Z, Su Y, Qin H, Zheng Y, Zhang B, Gao L, Chen Z, Huang H, Wang X and Sun Q. PCDH7 inhibits the formation of homotypic cell-in-cell structure. Front Cell Dev Biol 2020; 8: 329.

[13] Ning X, Luo T, Chen Z and Sun Q. The physics for the formation of cell-in-cell structures. Curr Mol Med 2015; 15: 867-872.
[14] Sun Q, Luo T, Ren Y, Florey O, Shirasawa S, Sasazuki T, Robinson DN and Overholtzer M. Competition between human cells by entosis. Cell Res 2014; 24: 1299-1310.
[15] Wang M, Niu Z, Qin H, Ruan B, Zheng Y, Ning X, Gu S, Gao L, Chen Z, Wang X, Huang H, Ma L and Sun Q. Mechanical ring interfaces between adherens junction and contractile actomyosin to coordinate entotic cell-in-cell formation. Cell Rep 2020; 32: 108071.
[16] Wang D, Zhang L, Hu A, Wang Y, Liu Y, Yang J, Du N, An X, Wu C and Liu C. Loss of 4.1N in epithelial ovarian cancer results in EMT and matrix-detached cell death resistance. Protein Cell 2021; 12: 107-127.
[17] Bozkurt E, Düssmann H, Salvucci M, Cavanagh BL, Van Schaeybroeck S, Longley DB, Martin SJ and Prehn JHM. TRAIL signaling promotes entosis in colorectal cancer. J Cell Biol 2021; 220: e202010030.
[18] Mackay HL, Moore D, Hall C, Birkbak NJ, Jamal-Hanjani M, Karim SA, Phatak VM, Piñon L, Morton JP, Swanton C, Le Quesne J and Muller PAJ. Genomic instability in mutant p53 cancer cells upon entotic engulfment. Nat Commun 2018; 9: 3070.
[19] Liang J, Niu Z, Zhang B, Yu X, Zheng Y, Wang C, Ren H, Wang M, Ruan B, Qin H, Zhang X, Zheng Y, Gu S, Sai X, Tai Y, Gao L, Ma L, Chen Z, Huang H, Wang X and Sun Q. p53-dependent elimination of aneuploid mitotic offspring by entosis. Cell Death Differ 2021; 28: 799-813.
[20] Ruan B, Zhang B, Chen A, Yuan L, Liang J, Wang M, Zhang Z, Fan J, Yu X, Zhang X, Niu Z, Zheng Y, Gu S, Liu X, Du H, Wang J, Hu X, Gao L, Chen Z, Huang H, Wang X and Sun Q. Cholesterol inhibits entotic cell-in-cell formation and actomyosin contraction. Biochem Biophys Res Commun 2018; 495: 1440-1446.
[21] Ruan B, Wang C, Chen A, Liang J, Niu Z, Zheng Y, Fan J, Gao L, Huang H, Wang X and Sun Q. Expression profiling identified IL-8 as a regulator of homotypic cell-in-cell formation. BMB Rep 2018; 51: 412-417.
[22] Liang J, Fan J, Wang M, Niu Z, Zhang Z, Yuan L, Tai Y, Chen Z, Song S, Wang X, Liu X, Huang H and Sun Q. CDKN2A inhibits formation of homotypic cell-in-cell structures. Oncogenesis 2018; 7: 50.
[23] Su Y, Huang H, Luo T, Zheng Y, Fan J, Ren H, Tang M, Niu Z, Wang C, Wang Y, Zhang Z, Liang J, Ruan B, Gao L, Chen Z, Melino G, Wang X and Sun Q. Cell-in-cell structure mediates in-cell killing suppressed by CD44. Cell Discov 2022; 8: 35.
[24] Wang S, Li L, Zhou Y, He Y, Wei Y and Tao A. Heterotypic cell-in-cell structures in colon cancer can be regulated by IL-6 and lead to tumor immune escape. Exp Cell Res 2019; 382: 111447.
[25] Galluzzi L, Vitale I, Aaronson SA, Abrams JM, Adam D, Agostinis P, Alnemri ES, Altucci L, Amelio I, Andrews DW, Annicchiarico-Petruzzelli M, Antonov AV, Arama E, Baehrecke EH, Barlev NA, Bazan NG, Bernassola F, Bertrand MJM, Bianchi K, Blagosklonny MV, Blomgren K, Borner C, Boya P, Brenner C, Campanella M, Candi E, Carmona-Gutierrez D, Cecconi F, Chan FK, Chandel NS, Cheng EH, Chipuk JE, Cidlowski JA, Ciechanover A, Cohen GM, Conrad M, Cubillos-Ruiz JR, Czabotar PE, D'Angiolella V, Dawson TM, Dawson VL, De Laurenzi V, De Maria R, Debatin KM, DeBerardinis RJ, Deshmukh M, Di Daniele N, Di Virgilio F, Dixit VM, Dixon SJ, Duckett CS, Dynlacht BD, El-Deiry WS, Elrod JW, Fimia GM, Fulda S, García-Sáez AJ, Garg AD, Garrido C, Gavathiotis E, Golstein P, Gottlieb E, Green DR, Greene LA, Gronemeyer H, Gross A, Hajnoczky G, Hardwick JM, Harris IS, Hengartner MO, Hetz C, Ichijo H, Jäättelä M, Joseph B, Jost PJ, Juin PP, Kaiser WJ, Karin M, Kaufmann T, Kepp O, Kimchi A, Kitsis RN, Klionsky DJ, Knight RA, Kumar S, Lee SW, Lemasters JJ, Levine B, Linkermann A, Lipton SA, Lockshin RA, López-Otín C, Lowe SW, Luedde T, Lugli E, MacFarlane M, Madeo F, Malewicz M, Malorni W, Manic G, Marine JC, Martin SJ, Martinou JC, Medema JP, Mehlen P, Meier P, Melino S, Miao EA, Molkentin JD, Moll UM, Muñoz-Pinedo C, Nagata S, Nuñez G, Oberst A, Oren M, Overholtzer M, Pagano M, Panaretakis T, Pasparakis M, Penninger JM, Pereira DM, Pervaiz S, Peter ME, Piacentini M, Pinton P, Prehn JHM, Puthalakath H, Rabinovich GA, Rehm M, Rizzuto R, Rodrigues CMP, Rubinsztein DC, Rudel T, Ryan KM, Sayan E, Scorrano L, Shao F, Shi Y, Silke J, Simon HU, Sistigu A, Stockwell BR, Strasser A, Szabadkai G, Tait SWG, Tang D, Tavernarakis N, Thorburn A, Tsujimoto Y, Turk B, Vanden Berghe T, Vandenabeele P, Vander Heiden MG, Villunger A, Virgin HW, Vousden KH, Vucic D, Wagner EF, Walczak H, Wallach D, Wang Y, Wells JA, Wood W, Yuan J, Zakeri Z, Zhivotovsky B, Zitvogel L, Melino G and Kroemer G. Molecular mechanisms of cell death: recommendations of the nomenclature committee on cell death 2018. Cell Death Differ 2018; 25: 486-541.
[26] Su Y, Ren H, Tang M, Zheng Y, Zhang B, Wang C, Hou X, Niu Z, Wang Z, Gao X, Gao L, Jiang H, Chen Z, Luo T and Sun Q. Role and dynamics of vacuolar pH during cell-in-cell mediated death. Cell Death Dis 2021; 12: 119.

[27] Overholtzer M, Mailleux AA, Mouneimne G, Normand G, Schnitt SJ, King RW, Cibas ES and Brugge JS. A nonapoptotic cell death process, entosis, that occurs by cell-in-cell invasion. Cell 2007; 131: 966-979.
[28] Benseler V, Warren A, Vo M, Holz LE, Tay SS, Le Couteur DG, Breen E, Allison AC, van Rooijen N, McGuffog C, Schlitt HJ, Bowen DG, McCaughan GW and Bertolino P. Hepatocyte entry leads to degradation of autoreactive CD8 T cells. Proc Natl Acad Sci U S A 2011; 108: 16735-16740.
[29] Sun Q and Chen W. Cell-in-cell: an emerging player in COVID-19 and immune disorders. Natl Sci Open 2022; 1: 20220001.
[30] Zhang Z, Zheng Y, Niu Z, Zhang B, Wang C, Yao X, Peng H, Franca DN, Wang Y, Zhu Y, Su Y, Tang M, Jiang X, Ren H, He M, Wang Y, Gao L, Zhao P, Shi H, Chen Z, Wang X, Piacentini M, Bian X, Melino G, Liu L, Huang H and Sun Q. SARS-CoV-2 spike protein dictates syncytium-mediated lymphocyte elimination. Cell Death Differ 2021; 28: 2765-2777.
[31] Ni C, Huang L, Chen Y, He M, Hu Y, Liu S, Fang X, Li J, Sun Q and Wang X. Implication of cell-in-cell structures in the transmission of HIV to epithelial cells. Cell Res 2015; 25: 1265-1268.
[32] Ni C, Chen Y, Zeng M, Pei R, Du Y, Tang L, Wang M, Hu Y, Zhu H, He M, Wei X, Wang S, Ning X, Wang M, Wang J, Ma L, Chen X, Sun Q, Tang H, Wang Y and Wang X. In-cell infection: a novel pathway for Epstein-Barr virus infection mediated by cell-in-cell structures. Cell Res 2015; 25: 785-800.
[33] Sun Q, Huang H and Overholtzer M. Cell-in-cell structures are involved in the competition between cells in human tumors. Mol Cell Oncol 2015; 2: e1002707.
[34] Mackay HL and Muller PAJ. Biological relevance of cell-in-cell in cancers. Biochem Soc Trans 2019; 47: 725-732.
[35] Fan J, Fang Q, Yang Y, Cui M, Zhao M, Qi J, Luo R, Du W, Liu S and Sun Q. Role of heterotypic neutrophil-in-tumor structure in the prognosis of patients with buccal mucosa squamous cell carcinoma. Front Oncol 2020; 10: 541878.
[36] Chen YH, Wang S, He MF, Wang Y, Zhao H, Zhu HY, Yu XM, Ma J, Che XJ, Wang JF, Wang Y and Wang XN. Prevalence of heterotypic tumor/immune cell-in-cell structure in vitro and in vivo leading to formation of aneuploidy. PLoS One 2013; 8: e59418.
[37] Huang H, He M, Zhang Y, Zhang B, Niu Z, Zheng Y, Li W, Cui P, Wang X and Sun Q. Identification and validation of heterotypic cell-in-cell structure as an adverse prognostic predictor for young patients of resectable pancreatic ductal adenocarcinoma. Signal Transduct Target Ther 2020; 5: 246-248.
[38] Zhang X, Niu Z, Qin H, Fan J, Wang M, Zhang B, Zheng Y, Gao L, Chen Z, Tai Y, Yang M, Huang H and Sun Q. Subtype-based prognostic analysis of cell-in-cell structures in early breast cancer. Front Oncol 2019; 9: 895.
[39] Ruan B, Niu Z, Jiang X, Li Z, Tai Y, Huang H and Sun Q. High frequency of cell-in-cell formation in heterogeneous human breast cancer tissue in a patient with poor prognosis: a case report and literature review. Front Oncol 2019; 9: 1444.
[40] Hayashi A, Yavas A, McIntyre CA, Ho YJ, Erakky A, Wong W, Varghese AM, Melchor JP, Overholtzer M, O'Reilly EM, Klimstra DS, Basturk O and Iacobuzio-Donahue CA. Genetic and clinical correlates of entosis in pancreatic ductal adenocarcinoma. Mod Pathol 2020; 33: 1822-1831.
[41] Almangush A, Mäkitie AA, Hagström J, Haglund C, Kowalski LP, Nieminen P, Coletta RD, Salo T and Leivo I. Cell-in-cell phenomenon associates with aggressive characteristics and cancer-related mortality in early oral tongue cancer. BMC Cancer 2020; 20: 843.
[42] Schwegler M, Wirsing AM, Schenker HM, Ott L, Ries JM, Buttner-Herold M, Fietkau R, Putz F and Distel LV. Prognostic value of homotypic cell internalization by nonprofessional phagocytic cancer cells. Biomed Res Int 2015; 2015: 359392.
[43] Wang Y, Niu Z, Zhou L, Zhou Y, Ma Q, Zhu Y, Liu M, Shi Y, Tai Y, Shao Q, Ge J, Hua J, Gao L, Huang H, Jiang H and Sun Q. Subtype-based analysis of cell-in-cell structures in esophageal squamous cell carcinoma. Front Oncol 2021; 11: 670051.

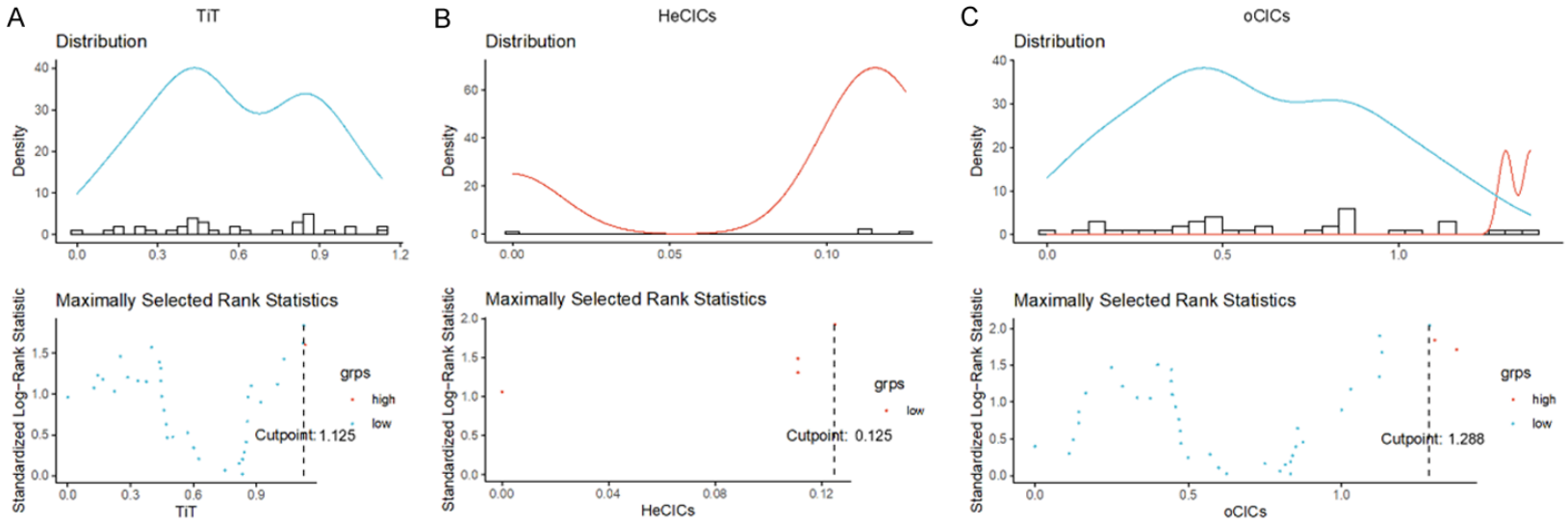

Figure S1. Selection of the optimal cutpoints for different CICs. The maximally selected rank statistics were used to select the optimal cutpoint for TiT (A), heCICs (B) and oCICs (C), respectively, by the surv_cutpoint function of the "survminer" R package.

Table S1. Association of CICs subtypes with the overall survival of patients with NSCLC

CICs	Survival time (mon)	Valid n (%)	Low n (%)	High n (%)	*P* value
TiT	<43	84 (51.5)	78 (92.9)	6 (7.1)	0.016
	≥43	79 (48.5)	66 (83.5)	13 (16.5)	
TiM	<43	84 (51.5)	4 (4.8)	80 (95.2)	0.015
	≥43	79 (48.5)	0 (0.0)	79 (100.0)	
LiT	<43	84 (51.5)	5 (6.0)	79 (94.0)	0.142
	≥43	79 (48.5)	1 (1.3)	78 (98.7)	
MiT	<43	84 (51.5)	0 (0.0)	84 (100.0)	0.016
	≥43	79 (48.5)	6 (7.6)	73 (92.4)	
HeCICs	<43	84 (51.5)	77 (91.7)	7 (8.3)	0.194
	≥43	79 (48.5)	66 (83.5)	13 (16.5)	
oCICs	<43	84 (51.5)	73 (86.9)	11 (13.1)	0.022
	≥43	79 (48.5)	73 (92.4)	6 (7.6)	

Mon: month. Tumor-in-tumor (TiT) Low: <1.125 CICs/mm^2, High: ≥1.125 CICs/mm^2; heterotypic CICs (HeCICs) Low: <0.125 CICs/mm^2, High: ≥0.125 CICs/mm^2; overall CICs (oCICs) Low: <1.288 CICs/mm^2, High: ≥1.288 CICs/mm^2; tumor-in-macrophage (TiM), lymphocyte-in-tumor (LiT) and macrophage-in-tumor (MiT), No: 0 CICs/mm^2; Yes: >0 CICs/mm^2. Spearman rank test was used to determine the association between variables.